

On secondary instabilities generating footbridges between spiral vortex flow

This content has been downloaded from IOPscience. Please scroll down to see the full text.

2014 Fluid Dyn. Res. 46 025503

(<http://iopscience.iop.org/1873-7005/46/2/025503>)

View [the table of contents for this issue](#), or go to the [journal homepage](#) for more

Download details:

IP Address: 193.170.138.132

This content was downloaded on 11/02/2014 at 09:18

Please note that [terms and conditions apply](#).

On secondary instabilities generating footbridges between spiral vortex flow

Sebastian A Altmeyer

Institute of Science and Technology Austria (IST Austria), A-3400 Klosterneuburg,
Austria Max-Planck-Institute for Dynamic and Self-Organization, D-37073 Göttingen,
Germany

E-mail: sebastian_altmeyer@t-online.de

Received 25 March 2013

Accepted for publication 10 January 2014

Published 5 February 2014

Communicated by E Knobloch

Abstract

This work investigates the transition between different traveling helical waves (spirals, SPIs) in the setup of differentially independent rotating cylinders. We use direct numerical simulations to consider an infinite long and periodic Taylor–Couette apparatus with fixed axial periodicity length. We find so-called mixed-cross-spirals (MCSs), that can be seen as nonlinear superpositions of SPIs, to establish stable *footbridges* connecting SPI states. While bridging the bifurcation branches of SPIs, the corresponding contributions within the MCS vary continuously with the control parameters. Here discussed MCSs presenting footbridge solutions start and end in *different* SPI branches. Therefore they differ significantly from the already known MCSs that present bypass solutions (Altmeyer and Hoffmann 2010 *New J. Phys.* **12** 113035). The latter start and end in the *same* SPI branch, while they always bifurcate out of those SPI branches with the larger mode amplitude. Meanwhile, these only appear within the coexisting region of both SPIs. In contrast, the footbridge solutions can also bifurcate out of the minor SPI contribution. We also find they exist in regions where only one of the SPIs contributions exists. In addition, MCS as footbridge solution can appear either stable or unstable. The latter detected *transient* solutions offer similar spatio-temporal characteristics to the flow establishing stable footbridges. Such transition processes are interesting for pattern-forming systems in general because they accomplish transitions between traveling waves of different azimuthal wave numbers and have not been described in the literature yet.

(Some figures may appear in color only in the online journal)

 Online supplementary data available from stacks.iop.org/FDR/46/025503/mmedia

Nomenclature

We use the following abbreviations for the different flow states discussed in this paper:

| | |
|-------|-----------------------|
| CCF | circular Couette flow |
| TVF | Taylor vortex flow |
| SPI | spiral vortex flow |
| R-SPI | right-winding SPI |
| L-SPI | left-winding SPI |
| CSPI | cross-spiral |
| RIB | ribbon |
| MCS | mixed-cross-spiral |
| MRIB | mixed-ribbon |

We denote R-SPIs with red triangles (▼), L-SPIs with orange triangles (▲), RIBs with green lozenges (◆) and MCSs with maroon squares (■).

1. Introduction

The flow of a fluid in between rotating cylinders is a prototypical example for pattern forming systems. Since the first studies by Taylor (1923) numerous structures with different topology appearing in such a system have been studied extensively during recent decades, experimentally, theoretically, as well as numerically (Jones 1984, DiPrima *et al* 1985, Andereck *et al* 1986, Iooss 1986, Nagata 1986, Golubitsky *et al* 1988, Langford *et al* 1988, Chossat and Iooss 1994, Tagg 1994, Hoffmann and Lücke 2000, Marques and Lopez 2002, Altmeyer and Hoffmann 2010). Various solutions and bifurcation scenarios just as transitions between fully developed states have been documented.

Here we investigate flow structures under Taylor–Couette geometry (Tagg 1994), where the basic state is given by the circular-Couette flow (CCF). To that end we consider an infinitely long and periodic Taylor–Couette apparatus with fixed axial periodicity length. These reductions result in limitations. Either comparison with experimental results is difficult and phenomena such as Eckhaus instabilities, concerning bifurcations between states with different axial wavelength are excluded.

The most important critical states are both primary bifurcating structures, the rotationally symmetric Taylor vortex flow (TVF) with toroidally closed vortices and the oscillatory spiral vortex flow (SPI) with open, helicoidal vortices. It follows that the latter occurs as symmetry degenerated, oppositely traveling, right-winding (R-SPI) or left-winding spiral (L-SPI) being mirror images of each other (Hoffmann and Lücke 2000). They are determined by their helicity and azimuthal wave number or, alternatively, by their pitch (Altmeyer and Hoffmann 2010).

One typical class of transitions is between these two topological different structures that are mediated by secondarily bifurcating states, namely the wavy Taylor vortices and wavy spirals (Swinney and Gollub 1981, Swift *et al* 1982, Jones 1984, Golubitsky *et al* 1988, Hoffmann *et al* 2009).

On the other hand transitions between helical SPIs with the *same* azimuthal wave number but *different* pitches was observed to be performed via secondarily bifurcating cross spirals (CSPIs) (Pinter *et al* 2006). Herein the bifurcation goes over the solution of primary bifurcating ribbons (RIBs) (Chossat and Iooss 1994, Pinter *et al* 2008). These can be seen as a nonlinear superposition of two mirror-symmetric SPIs, i.e. L- and R-SPIs with *same* azimuthal wave number and *identical* mode amplitudes but *opposite* helicity (i.e. opposite pitches $\pm p$, equation (7)).

We here investigate mixed-cross-spirals (MCSs) which offer a *direct* way to bridge SPI solution branches with *different* helicities and *different* pitches (i.e. different azimuthal wave numbers) without making a detour over any other primary bifurcating solution. Therein a special case is the appearance of MCSs as *bypass* solution. These present a way to connect the *same* SPI solution branch (starting and ending in it) via secondary forward bifurcations as already discussed in Altmeyer and Hoffmann (2010). Moreover, such bridge solutions that connect states with same helicity but different azimuthal wavenumber (i.e. pitch) were investigated in Deguchi and Altmeyer (2013).

While theoretically all combinations of azimuthal wave numbers are possible for MCSs to establish footbridges, numerically we only observed selected combinations. We find these footbridge solutions exist as stable and unstable flow states. To find several of these solutions we restricted our code to subspaces due to permission of only selected modes. Note that any solution that is stable in any selected subspace may be unstable in full space or another subspace with less constrictions. Moreover, any solution found in subspace is also a physical solution. Exploiting the confinement, we also find MCSs appear as short-live-time *transient* flows due to an externally applied artificial generation scenario and then let fall some constrictions. For example, first just allow to a subspace for SPI and then relax some confinement to allow to a subspace of MCS.

Presented processes here are interesting for pattern forming systems in general because they accomplish transitions between traveling waves of both different azimuthal wave numbers and propagation direction. In principle the MCSs can be seen as nonlinear superpositions of two SPIs with different helicity and different azimuthal wave number M . Thus, such transitions mainly involve the Fourier mode subspaces of the participating SPI structures.

The paper is roughly subdivided into four parts. Following the introduction, we briefly present the system, the numerical methods in section 2 and classification of the investigated solutions in section 3. This is followed by the main part in section 4 and section 5 elucidating the bifurcation scenario and spatio-temporal behavior for MCSs establishing footbridge solutions. Here we also illustrate the similarity between both findings, stable and transient MCSs, in which the latter were observed as short-live-time flow due to an artificial generation scenario. Finally, section 6 provides conclusion and discussion of the main results.

2. System and theoretical description

Consider the flow driven in the annular gap between two independently rotating cylinders of length L . The inner cylinder of radius R_i rotates at angular speed Ω_i and the outer cylinder of radius R_o rotates at angular speed Ω_o . The fluid in the annulus is considered to be Newtonian, isothermal and incompressible with kinematic viscosity ν . Using the gap width $R_o - R_i$ as the length scale and the radial diffusion time $(R_o - R_i)^2/\nu$ as the time scale, the non-dimensional Navier–Stokes equations governing the flow read

$$\partial_t \mathbf{u} + (\mathbf{u} \cdot \nabla) \mathbf{u} = -\nabla p + \nabla^2 \mathbf{u}, \quad \nabla \cdot \mathbf{u} = 0, \quad (1)$$

where $\mathbf{u} = (u, v, w)$ is the velocity in cylindrical coordinates (r, θ, z) .

In the present work, we assume axial periodic boundary conditions, determining the axial wave number that we shall fix, $k = 3.927$, and the radius ratio R_i/R_o is also fixed to 0.883. The selection of this axial wave number is motivated due to experimental findings, in particular for the here chosen radius ratio. Under these conditions the system is governed by only two

Table 1. Isotropy subgroups of discussed fluid states.

| Solution | Isotropy subgroup |
|-----------|---------------------------------------|
| CCF | $SO(2) \times O(2)$ |
| TVF | $SO(2) \times Z_2(\kappa)$ |
| SPI | $\widetilde{SO}(2) \times \Delta$ |
| RIB | $Z_2(\kappa) \oplus Z_2(\pi, \pi)$ |
| MCS, CSPI | $\widetilde{SO}(2) \times \Delta$ |
| MRIB | $Z_2(\kappa) \oplus Z_2(\pi, \gamma)$ |

$\kappa \in O(2)$ is the flip $z \rightarrow -z$ along the cylindrical axis,

$\alpha \in SO(2)$ is a rotation in the azimuthal plane,

$\Delta = \{(\alpha, -\alpha) \in SO(2)\}$,

$\widetilde{SO}(2) = \{(\psi, -\psi) \in O(2) \times SO(2)\}$,

$\widetilde{SO}(2) = \{((\psi, -\psi), (\beta, -\beta)) \in O(2) \times SO(2)\}$

parameters, the inner and outer Reynolds numbers

$$Re_1 = \Omega_i R_i (R_o - R_i) / \nu \quad \text{and} \quad Re_2 = \Omega_o R_o (R_o - R_i) / \nu. \quad (2)$$

Likewise the boundary conditions at the cylinder surfaces are no-slip, with $\mathbf{u}(r_i, \theta, z, t) = (0, Re_1, 0)$ and $\mathbf{u}(r_o, \theta, z, t) = (0, Re_2, 0)$, where the non-dimensional inner and outer radii are $r_i = R_i / (R_o - R_i)$ and $r_o = R_o / (R_o - R_i)$. Throughout this paper Re_1 is hold fixed either to 200 or 370 and Re_2 varies within $[-900; 400]$.

The governing equations and the boundary conditions are invariant under time translation ϕ_τ , arbitrary rotations R_α about the axis, and translation T_β and flipping K_z along the cylindrical axis, generating the combined symmetry group $\Gamma = SO(2) \times O(2)$. The actions of these symmetries on the velocity are

$$\phi_\tau(\mathbf{u}, v, w)(r, \theta, z, t) = (\mathbf{u}, v, w)(r, \theta, z, t + \tau), \quad (3a)$$

$$R_\alpha(\mathbf{u}, v, w)(r, \theta, z, t) = (\mathbf{u}, v, w)(r, \theta + \alpha, z, t), \quad (3b)$$

$$K_z(\mathbf{u}, v, w)(r, \theta, z, t) = (\mathbf{u}, v, -w)(r, \theta, -z, t), \quad (3c)$$

$$T_\beta(\mathbf{u}, v, w)(r, \theta, z, t) = (\mathbf{u}, v, w)(r, \theta, z + \beta, t). \quad (3d)$$

Note, that this paper only discusses the infinitely long and periodic Taylor–Couette apparatus; there are some appreciable limitations: first of all it neglects all axial endwall effects and thus makes difficult the comparison with experimental results. Moreover, due to the fixed axial periodicity, phenomena such as Eckhaus instabilities concerning bifurcations between states with different axial wavelength are also excluded. Nevertheless, the solutions considered in the paper may play an important role in real experiments, depending on other system parameters such as radius ratio, aspect ratio and kind of endwalls used.

One can distinguish each of the different states described in this paper by their isotropy subgroups; that is by $SO(2) \times O(2)$ which leave the given state invariant. In table 1 we list the different isotropy subgroups for the main fluid states discussed in this paper following the notation in Golubitsky and Stewart (1986).

To the steady solutions, the CCF is invariant under all symmetries. TVF is invariant under all rotations $SO(2)$ and flips along the cylindrical axis $Z_2(\kappa)$.

To the periodic solutions, these all present rotating waves and thus they are invariant under Δ since a change of phase may be compensated for by rotating the cylinder. The SPI

is invariant under $\widetilde{SO}(2)$; a translation along the cylinder axis may be compensated for by rotation of the cylinder. RIB is invariant under composing flip K_z with discrete angle rotation of the cylinder by π . MCS is invariant under $\widetilde{SO}(2)$; only discrete translation along the cylinder axis combined with rotation of the cylinder keeps the solution invariant. Finally, mixed-ribbon (MRIB) differs from RIB due to $\pi \neq \gamma$.

2.1. Numerical methods

Numerical simulations have been done with our code ‘G2D2’ as presented in detail in Hoffmann *et al* (2009) which implements a Galerkin–Fourier expansion in two dimensions, θ and z , and finite differences of second order in r and of first order in t

$$f(r, \theta, z, t) = \sum_{m,n} f_{m,n}(r, t) e^{i(m\theta + nkz)}, \quad f \in \{u, v, w, p\}. \quad (4)$$

Here, $f_{m,n}(r, t)$ are the amplitudes of the m th azimuthal and the n th axial Fourier mode. Their variation in the two variables r and t is determined using finite differences. For an adequate accuracy we choose $m_{\max} = 15 = n_{\max}$ and 31 points in radial direction.

Note that the decomposition (4) allows imposing constrictions during the numerical calculations by selecting subspaces of the full solutions. In practice this means that all Fourier-modes not allowed (exist) in the selected subspace are set to zero after each iteration. All solutions found in a subspace are also solutions of the full Navier–Stokes equations, and therefore represent physical flow states.

2.2. Characterization

In order to classify the structures, we shall refer to their significant Fourier mode (4) indices abbreviated with

$$(m, n) := f_{m,n} e^{i(m\theta + nkz)}, \quad f \in \{u, v, w, p\}. \quad (5)$$

The SPI is of special interest as it either presents start and end state for footbridges and also appears as an ingredient in the the footbridges itself.

SPIs show a combined symmetry under rotation and axial translation or time translation, where it follows that flow fields do not depend on θ, z, t separately but only on the phase combination (Pinter *et al* 2006) $\Phi := M\theta + Kz - \omega t$ such that $f(r, \theta, z, t) = F(r, \Phi)$. The spiral frequencies ω depend on the Reynolds numbers Re_1, Re_2 and on the azimuthal (M) and axial (K) wave numbers. The latter is given by $K = \pm k$, depending on the helicity of the respective spiral, i.e. $K > 0$ for (left-winding) L-SPI and $K < 0$ for (right-winding) R-SPI. R- and L-SPI, characterized by $K = K_R, M = M_R, \omega = \omega_R$ and $K = K_L, M = M_L, \omega = \omega_L$, respectively, are mirror-symmetric at mid-height ($z \rightarrow -z$), i.e. $\Phi_{L-SPI}(z, \theta, t) = \Phi_{R-SPI}(-z, \theta, t)$. Considering various $M_{R,L} \geq 1$, this yields $K_L = -K_R, M_L = M_R$ and $\omega_L = \omega_R$. The frequencies are positive since the spirals rotate into the same direction as the inner cylinder. This in turn implies that the phase of L-SPI propagates axially upward while the converse holds for the R-SPI—the location $z_0(\theta)$ of a particular phase value, say, $\Phi = 0$, at a fixed time t is given by

$$z_0 = -\frac{M}{K}\theta + \frac{\omega}{K}t. \quad (6)$$

Thus, for the reduced axial pitch p of a SPI follows:

$$p := \frac{z_0(2\pi) - z_0(0)}{\lambda} = -M \frac{k}{K} = -\text{sign}[K] M \quad (7)$$

which gives the number of axial periodicity lengths being covered while traveling in positive azimuthal direction along the helicoidal vortex tube once around the cylinder. Hence, $p\lambda/2\pi = -M/K$ is the slope of the lines of constant phase in the (θ, z) plane of an azimuthally unrolled cylindrical surface.

In this paper, we consider only vortex structures with the *same* axial wave number $k = 3.927$. To identify the different flow structures investigated here, we will use a combination of letters and numbers as follows: e.g. L1-SPI is a left-winding spiral with azimuthal wave number $M = 1$ (thus the pitch of it is given by $p = -1$ (7)) while R2-SPI stands for a R-SPI with azimuthal wave number $M = 2$ (thus $p = 2$), see figure 5. The symbols ‘L1’ and ‘R2’ correspond to the pitch of the SPI. In analogy, we will also characterize the MCS with both its, major (first) and minor (second) contribution, e.g. L1R2-MCS (R1L2-MCS) stands for an upward (downward) propagating flow state due to major L1 (R1) contribution, where it follows that the pattern is modulated due to the downward (upward) propagating minor R2 (L2) contribution.

3. Classification of MCS

Due to the absence of axial symmetry breaking effects, both oscillatory L- and R-SPIs are degenerated, i.e. L- and R-SPI with different helicity but the same azimuthal wave number bifurcates at a common threshold. Additionally the so-called RIB bifurcates with the SPIs. RIBs can be seen as a nonlinear superposition of two mirror symmetric SPIs. In axial direction they present a standing wave. The common threshold also holds for MCS exchanging major and minor SPI contributions, e.g. L3R4-MCS and its mirror image R3L4-MCS. So it suffices to present the results for only one type of the MCSs, the corresponding mirror-symmetric ones are meant to be included as well.

The Taylor–Couette system exhibits a large variety of possible transitions between different SPI branches. One of these is organized by the so-called CSPIs which mediate transition between SPIs with the *same* azimuthal wave number but opposite helicity, i.e. opposite pitch $\pm p$ (e.g. 2-CSPI in Pinter *et al* 2008). They can be seen as nonlinear superpositions of the participating spirals (L2-SPI and R2-SPI). Likewise, the secondarily bifurcating solutions of MCS can be seen as nonlinear superpositions of SPIs with *different* azimuthal wave numbers (e.g. L3-SPI and R4-SPI) and (in general) *different* helicity. In principle MCSs can bridge between solutions with either the same or different helicity. In this paper, we only focus on the latter, establishing footbridges between SPIs with different helicities. Footbridge solutions between SPIs with the same helical orientation have been discussed among others in Deguchi and Altmeyer (2013). The situation of *bypass* solution branches of MCS which starts and ends in the same SPI have already been investigated in detail (Altmeyer and Hoffmann 2010). Schematics of MCS that mediate the transition between SPIs of different M (e.g. L1-SPI \leftrightarrow L1R2-MCS \leftrightarrow L1R2-MRIB \leftrightarrow R2L1-MCS \leftrightarrow R2-SPI) are shown in figure 5. Before going into more details of this transition, we will explain the classification, terminology, some general properties and the most important results of the first type MCS (bypass). All MCSs are found to bifurcate *secondarily* out of a pure SPI state of one of both its contributions, from where they are generated. In the case of bypass solution there is some special behavior as discussed in detail in Altmeyer and Hoffmann (2010).

MCSs characterize very general flow structures exhibiting a broad class of solutions. Thus, the solution of CSPI can be seen as a special case of MCS with the *same* azimuthal wave numbers but different mode amplitudes. Having equal amplitudes, we define the RIB solution. On the other side, the same amplitudes but different azimuthal wave numbers

indicate the so-called MRIB (Altmeyer and Hoffmann 2010). Both, MCS as well as CSPI can be seen as nonlinear superpositions of oppositely traveling waves with continuously varying contributions. Thus, CSPIs (RIB) represent a special type of MCS (MRIB). Furthermore, RIB (MRIB) can be seen as a special type of CSPI (MCS) with equal amplitude contributions from L- and R-SPI.

To put the present work in the right context, we clarify the naming of the here-discussed MCSs as footbridges and the differences to the already known ones as bypass solutions (Altmeyer and Hoffmann 2010). MCSs are built of a nonlinear superposition of two SPIs with different helicity and pitch. While the bypass solutions bifurcate out and end in the *same* SPI branch (therefore the name ‘bypass’), the footbridge solution connects *different* SPI branches. Thus, the current study can be seen as a generalization of the older one.

4. Structural properties of MCS

In order to get an impression of the spatial shape of MCS, figure 1 presents either isosurfaces of the azimuthal vorticity $\eta = \partial_z u - \partial_t w$ (a) and horizontal cuts in (r, θ) plane (b) through the annulus at mid-height of an L3R5-MCS (2), and separate for both its contributions L3-SPI (1) and R5-SPI (3), respectively. Here, the choice of the L3R5-MCS is motivated by the fact that the composition of this state by two SPI contributions with difference in azimuthal wave number $\Delta M = 2$ (L3- and R5-) results in significantly better visibility of the setting (instead for only $\Delta M = 1$).

The L3R5-MCS in figure 1 consists of a stronger (major) L3 and a weaker (minor) R5 component obvious in the helical left-winding orientation of the L3R5-MCS. It follows that the vorticity maxima in both contributions L3 and R5, and therefore their contributions to the complete MCS structure, differ significantly (see caption for values of η and its maximum and minimum). The L3 contribution dominates the whole L3R5-MCS structure, and R5 portion only generates a weak modulation. In this case, the full structure propagates upwards, i.e. in positive axial direction, due to the major L3 component, whereas the modulation, minor R5 component, travels downwards (see online available material: movie1.avi and movie2.avi, available from stacks.iop.org/FDR/46/025503/mmedia). The difference in the azimuthal wave numbers is visible in (r, θ) plane in figure 1(b). The pure states, L3-SPI and R5-SPI, present three and five helical pairs of vortex tubes, respectively. Due to the dominance of the major L3 contribution in the L3R5-MCS, there are also three helical pairs of vortex tubes visible (figure 1(2)).

For local measures, we will use the azimuthal vorticity on the inner cylinder at two points symmetrically displaced about mid-plane, $\eta_- = \eta(r_1, 0, \Gamma/4, t)$ and $\eta_+ = \eta(r_1, 0, \Gamma/4, t)$. Figure 2 shows time series of η_{\pm} , and their corresponding PSDs for L3R5-MCS (top row), L3-SPI (middle row) and R5-SPI (bottom row) at $Re_1 = 200$ and $Re_2 = 0$. The time-series of η_{\pm} show a ‘simple’ periodic modulation for the pure states, L3-SPI and R5-SPI, respectively. This results in PSDs that each highlight one single characteristic frequency, ω_{L3-SPI} and ω_{R5-SPI} . Likewise, the time series of η_{\pm} for the L3R5-MCS looks more complicated, offering a mixture of both pure SPI contributions. The corresponding PSD shows both frequencies of the pure SPI states as dominant ones and various frequencies of its superposition as minor ones. Both frequencies for left- or right-winding contribution is dominant and depend on various other system parameters. As already discussed, L3R5-MCS propagates upwards, thus ω_{L3-SPI} is dominant, whereas ω_{R5-SPI} characterizes the downward directed modulation. But apart from this, further frequencies appear in the spectrum, due to nonlinear superposition. In detail, these can be identified as $2\omega_{L3-SPI} - \omega_{R5-SPI}$ and $\omega_{R5-SPI} - \omega_{L3-SPI}$.

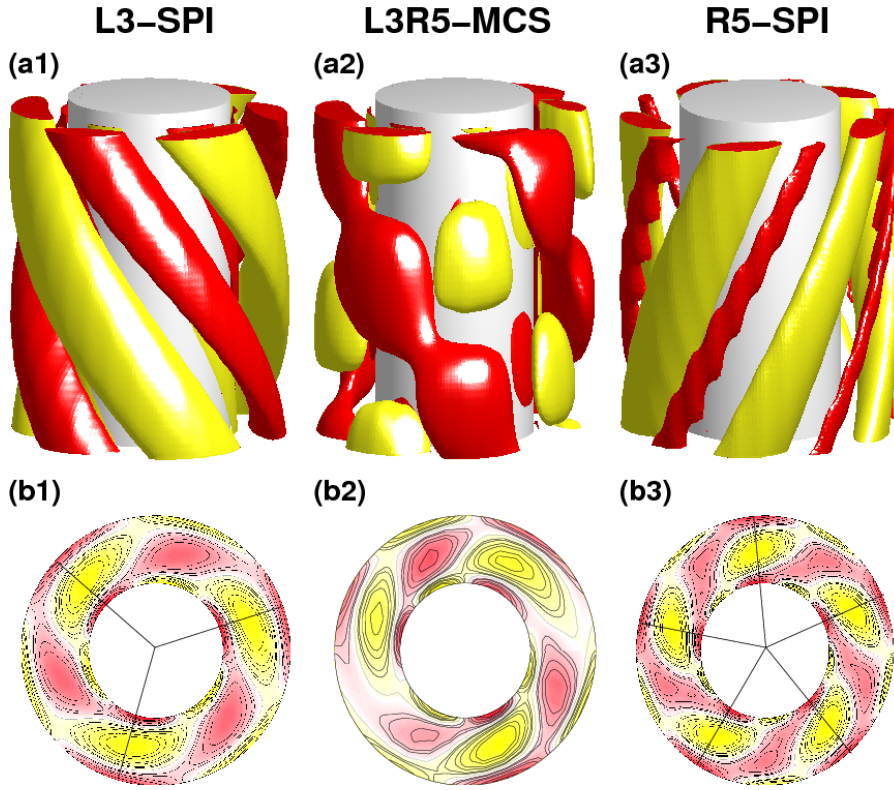


Figure 1. Isosurfaces (a) of azimuthal vorticity $\eta = \partial_z u - \partial_r w$ (isolevels shown for (a1) ± 70 [min, max] = $[-250, 250]$, (a2) ± 80 [310, -310], (a3) ± 40 [220, -220]) and horizontal cuts in (r, θ) plane at mid-height (b) of L3-SPI (1), L3R5-MCS (2) and R5-SPI (3) at $Re_1 = 200$ and $Re_2 = 0$. In axial direction, each isosurface plot covers one axial wavelength $2\pi/k$. (2) Displays the complete MCS structure and (1) and (3) depicts the separated contributions of the respective L3-SPI and R5-SPI component subspaces. Piecewise cuts in (b) are to guide the eye and help to indicate the symmetry in azimuth. Red (yellow) indicates positive (negative) isovorticity values. See also online available material movie1.avi and movie2.avi (available from stacks.iop.org/FDR/46/025503/mmedia).

Figure 3 shows phase portraits of L3-SPI, R5-SPI and L3R5-MCS on $(\eta_-, -\eta_+)$ and their corresponding two-dimensional Poincaré section for η_- on (u, η_+) , where $u := u(d/2, 0, \Gamma/2, t)$. The Poincaré section corresponds to $\eta_- = 0$. The phase portraits of both pure SPI clearly indicate the fact that these solutions are limit-cycle solutions. Otherwise the MCS exist on an other complex topology—a 2-torus. Thus its corresponding Poincaré section (figure 3(d)) presents a closed circle. For comparison, the two additional indicated points in the Poincaré section (figure 3(d)) correspond to limit-cycles of L3-SPI and R5-SPI, respectively.

5. Transition between SPIs

In the following, we will first give a brief review of the special case, MCS presenting bypass solutions bifurcating out and ending in the same SPI branch.

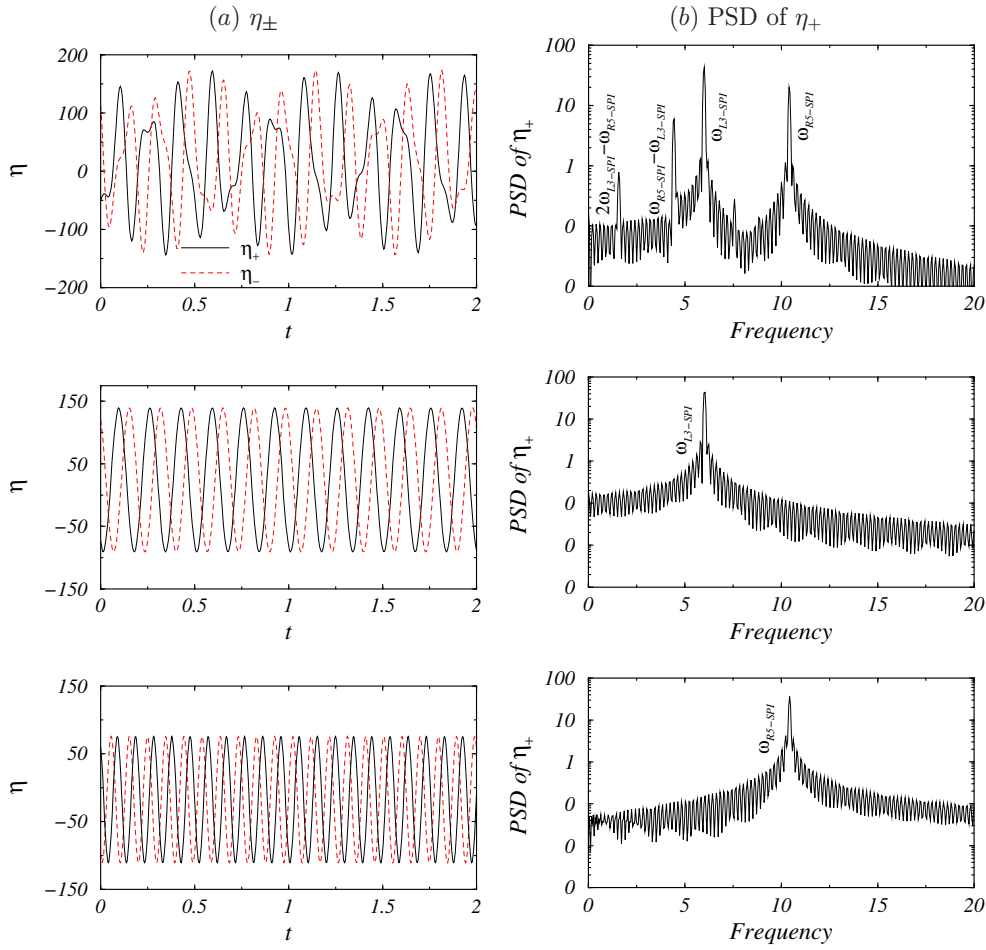


Figure 2. Time series (a) of $\eta_- = \eta(r_1, 0, -\Gamma/4, t)$ and $\eta_+ = \eta(r_1, 0, \Gamma/4, t)$, and their corresponding power spectral density (PSD) (b) for L3R5-MCS (top), L3-SPI (middle) and R5-SPI (bottom) at $Re_1 = 200$ and $Re_2 = 0$ (see figure 1).

5.1. MCS as bypass solution

Figure 4 shows a schematic for the appearance of MCS as bypass solution with suitable control parameter, say, e.g. Re_2 . Thereby, the azimuthal wave numbers are considered to be different $a \neq b$ (for $a = b$ see (Pinter *et al* 2008)). The most important points for all MCSs found in Altmeyer and Hoffmann (2010) to appear as bypass solution are:

- (i) These MCSs start and end in the same SPI branch.
- (ii) They only exist in regions, where both SPI contributions exist simultaneously.
- (iii) They always bifurcate out and end in that SPI contribution with the larger mode amplitude (major SPI contribution).
- (iv) While theoretically any combination of azimuthal wave numbers are possible, numerically only selected ones were observed. But note this also holds for MCSs establishing footbridges (e.g. the theoretical transition from L1-SPI \leftrightarrow R2-SPI as schematically presented in figure 5 could not be found numerically).

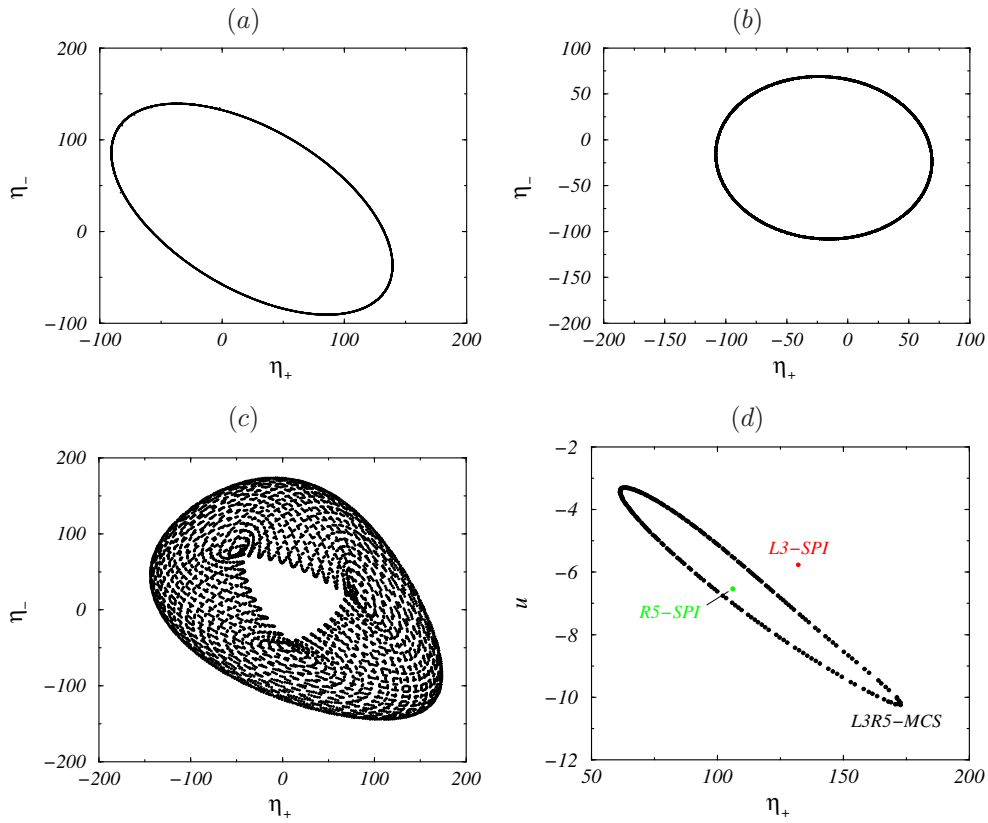


Figure 3. Phase portraits of (a) L3-SPI, (b) R5-SPI and (c) L3R5-MCS at $Re_1 = 200$ and $Re_2 = 0$ on (η_+, η_-) plane and corresponding two-dimensional Poincaré sections (d) (u, η_+) with $\eta_- = 0$, $u := u(d/2, 0, \Gamma/2, t)$ (see figure 2).

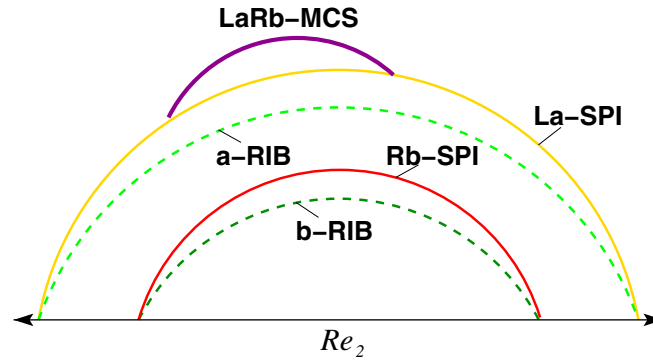


Figure 4. Schematics for the bifurcation of vortex flow amplitudes versus a suitable control parameter, e.g. Re_2 . SPI and RIB denote non-hysteretic solution branches that primary bifurcate out of the CCF state. The azimuthal wave numbers are considered to be different $a \neq b$. The MCS as bypass solution is indicated by the thick line starting and ending in the La-SPI solution branch which here gives the major SPI contribution.

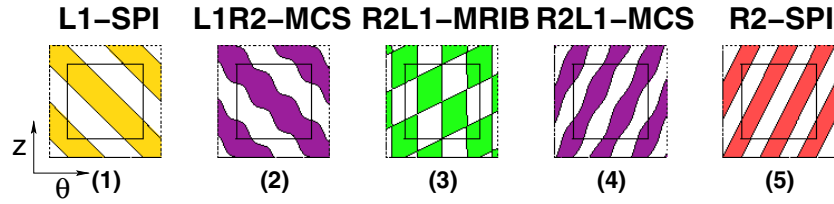


Figure 5. Schematics of several flow structures as indicated and discussed in this paper. The colored (gray shaded) regions denote radial outflow, $u > 0$ and the white ones indicate radial inflow, $u < 0$, respectively, in the plane of an unrolled cylinder surface in the annulus. The inner squares cover one azimuthal period 2π in horizontal direction and one axial wavelength $2\pi/k$ in vertical direction. For better visibility the structures are periodically continued slightly beyond these limits.

- (v) These MCSs can bifurcate either as stable solution out of stable SPI then losing its stability or as unstable solution to leave the stability of the pure state untouched.

In general at the onset, the amplitude of the respective MCS component is equal to the respective SPI (major contribution) amplitude, where it bifurcates out while the other component's (minor contribution) amplitude starts from zero. Note that different line styles in figure 4 do not say anything about the stability of the respective solutions. Besides, without any symmetry breaking effects, L- and R-SPI state and respective SPI contributions in the complete MCS are exchangeable. Drawing the MCS branch above the pure SPI branches does not say anything about magnitude of real mode amplitudes. Normally they are smaller in the MCS than in the SPI.

5.2. MCS establishing stable footbridges

In contrast to MCSs as bypass solution (Altmeyer and Hoffmann 2010) which have been only observed to exist *above* the bifurcation thresholds of both SPI contributions (see figure 4), the situation for MCS establishing footbridges becomes versatile. In the following, we discuss such a footbridge solution in detail for parameter path varying Re_2 at a fixed value $Re_1 = 370$. But before discussing this scenario in detail, we will schematically illustrate the transition.

5.2.1. Schematics of MCS. Figure 5 presents schematics for linear superposition of L1 ($p_1 = -1$) and R2 ($p_2 = 2$) SPI contributions with varying amplitude ratio. Note that we have chosen this example due to simplicity, although it could not be found in our simulations. The colored (gray shaded) regions denote radial outflow, $u > 0$ and the white ones indicate radial inflow, $u < 0$, respectively, in the plane of an unrolled cylinder surface in the annulus. The inner squares cover one azimuthal period 2π in horizontal direction and one axial wavelength $2\pi/k$ in vertical direction. Starting in (1) with a pure L1-SPI and increasing the R2 component, first leads to a left-winding L1R2-MCS (2) with the major azimuthal wave number $M = 1$, and the pitch $p = -1$. Equal L1 and R2 contributions in (3) yield to L1R2-/R2L1-MRIB with $p = 1/2$. In (4), the dominant R2 contribution establishes the right-winding characteristics of an R2L1-MCS. Finally, (5) shows a pure R2-SPI with vanishing L1 component. For both MCS states (2) and (4) hold similarly: the major SPI contribution determines the propagation direction of the whole structure, while the minor SPI contribution produces a modulation that is oppositely directed; thus the whole structure propagates upward (downward) in (2) ((4)) due to major L1 (R2) component. The spatio-temporal behavior of

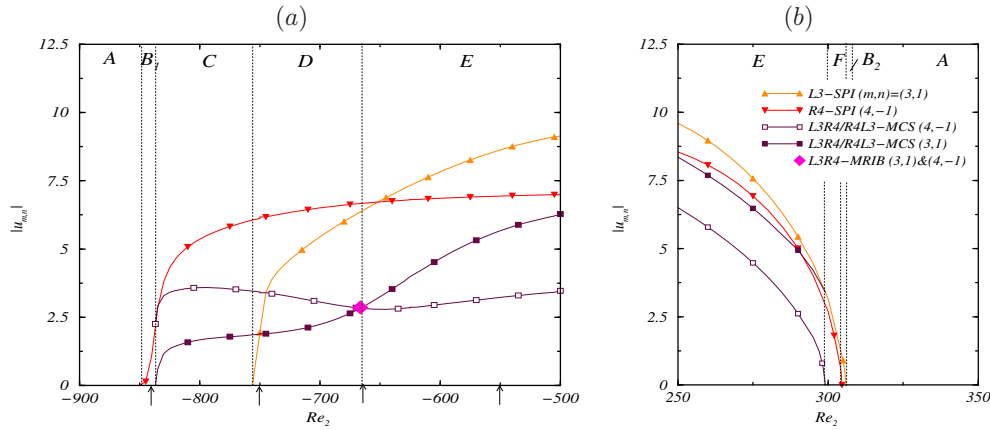


Figure 6. Bifurcation diagrams of the radial velocity amplitude $|u_{m,n}|$ at mid-gap for stable MCS as footbridge solution between two SPI states with different helicity at $Re_1 = 370$. (from left to right) R4L3-MCS (\square) bifurcating out of R4-SPI (\blacktriangledown), changing over R4L3-/L3R4-MRIB (\blacklozenge) into L3R4-MCS (\blacksquare) ending in L3-SPI (\blacktriangle). Due to complexity of this figure we want to refer to schematics in figure 11, that show an overall picture of different states and bifurcations. See text for detailed information. Arrows below abscissa mark those Re_2 for the present snapshots in that figure 7.

MCS exhibits aspects of both, SPI and RIB. Usually, all (vertical and horizontal) $\Phi = 0$ phase lines rotate in the same direction as the inner cylinder. In contrast to RIB states with horizontal pinned phase lines at distinct $z = \text{const.}$ positions the phase lines for MRIB are not—they have a finite slope (see finite pitch $p = 1/2$ in (3)). Instead the phase lines propagate axially due to their finite slope and the rotation of the complete pattern.

5.2.2. Bifurcation scenario. In this subsection we elucidate the bifurcation scenario of MCS as footbridge solutions exemplarily focusing on the transition between 3-SPI and 4-SPI. Figure 6 illustrates the bifurcation branches of L3-SPI (\blacktriangle), R4-SPI (\blacktriangledown), R4L3-MCS (\square) and L3R4-MCS (\blacksquare). For the here used control parameters the bifurcation order (out of CCF) of 3-SPI and 4-SPI depends on Re_2 . Thus, for strong counter-rotation (in figure 6(a) from left to right), first the 4-SPI and later the 3-SPI bifurcates out of CCF, while the sequence of bifurcation is reversed for co-rotating cylinders (figure 6(b)). Resulting in the solution branches (here for characteristic dominant mode amplitudes, i.e. (3,1) and (4, -1)) crosses at Re_2 about -654 . Note, that (i) all presented branches do not say anything about the stability of the respective solutions and (ii) SPI and RIB bifurcate at a common threshold. The latter and the branches of other solutions with $M \leq 2$ which also exist for these parameters are not of interest here and are therefore neglected in the figure due to better visibility.

We start the discussion of the bifurcation scenario presented in figure 6(a) on the left side in strong counter-rotating region A with basic state, CCF. For MCS, we captured both the major and the minor mode components, i.e. (3,1) and (4, -1) for R4L3-MCS and L3R4-MCS, respectively. At Re_2 about -850 (region B_1) first the R4-SPI (together with 4-RIB) bifurcates primarily out of the CCF (note that all RIBs are neglected due to better visibility). With increasing Re_2 , at about -837.5 the R4L3-MCS solution bifurcates secondarily out of the R4-SPI. Note this is significantly *below* the 3-SPI solution threshold. It follows that the major R4 contribution arises out of the R4-SPI branch while the minor L3 contribution of L3-SPI emerges from zero. At Re_2 about -756 also the L3-SPI bifurcates out of the CCF

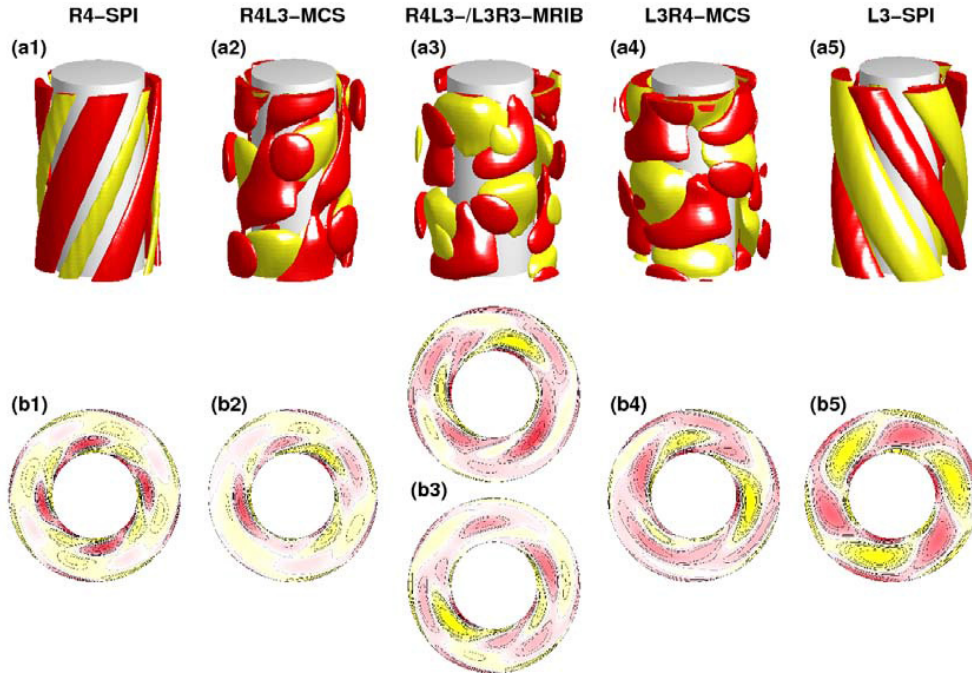


Figure 7. Snapshots of isosurfaces (a) of the azimuthal vorticity $\eta = \pm 80$ [min, max] = $[-340, 340]$ and (b) horizontal cuts in (r, θ) plane at mid-height, $z = 0$, (1,2,4,5) and $z = \pm\Gamma/2$ (3) for several flow structures at $Re_1 = 370$ and different Re_2 (1) -840 , (2) -750 , (3) -666.7 , (4) -550 and (5) -305.3 during the transition from R4-SPI to L3-SPI (see labels on top), as presented in figure 6 (see arrows below abscissa) (yellow (light gray)) denotes maximal inflow and red (dark gray) maximal outflow, respectively.

(region D). Further increasing Re_2 , the amplitude ratio $|u_{4,-1}/u_{3,1}|$ decreases, but first remains smaller than 1 (characterizing R4L3-MCS) while both major and minor mode amplitudes approach each other, i.e. the modulations of R4L3-MCS decrease (see figure 7). In regions C and D the whole structure is still downward propagating due to major R4 contribution. The minor L3 contribution just results in an upward propagating modulation. A point of special interest is at Re_2 about -666.5 , where the dominant mode amplitudes of both SPI contributions are identical presenting a R4L3-/L3R4-MRIB state. Hereafter, on further increasing Re_2 , the structural properties are changed in region E. Now the amplitude ratio $|u_{4,-1}/u_{3,1}|$ is larger than 1 characterizing an L3R4-MCS, which is upward propagating due to the major L3 contribution and modulated by the minor R4 contribution (see also movie5.avi, available from stacks.iop.org/FDR/46/025503/mmedia). Apart from changing the magnitude of SPI contributions in the MCS (between regions D and E) this L3R4-MCS is conserved for increasing Re_2 over a wide range of Reynolds numbers ($-644.8; 298.7$) (neglected as not of interest). Finally the MCS branch ends in the L3-SPI solution branch at Re about 306.4 (see figure 6(b)).

Note, for the sake of visibility we presented only one of the two respective SPI branches, namely L3-SPI and R4-SPI. In the absence of symmetry breaking effects, the connection from L4-SPI to the R3-SPI branch via MCS state looks exactly the same by changing L- and R-SPI contributions. Moreover, the branches presented here do not say anything about the stability of the respective solutions in full space or other subspaces. Meanwhile, solutions

which also exist for these parameters with either $M \leq 2$ and corresponding RIB having the common threshold as SPI are not of interest and therefore also neglected in the figure due better visibility. Symbols are just to guide the eye; the numerical calculations have been done for significantly more values.

5.2.3. Spatio-temporal characteristics. The arrows in figure 6 mark Reynolds numbers, where we made the five snapshots of figure 7 that depict (a) isosurfaces and (b) horizontal cuts of the azimuthal vorticity η in (r, θ) (at mid-height, $z = 0$, but (3) at $\Gamma/4$ and $-\Gamma/4$, respectively). The snapshot sequence illustrates the structural changes of the footbridge solution during the transformation from R4-SPI to L3-SPI. In the axial direction, each isosurface plot (a) covers one axial wavelength. Starting with a pure R4-SPI (figure 7(1)) the azimuthal wavenumber $m = 4$ is obvious, the horizontal cut in (r, θ) clearly indicates four pairs of vortex tubes. This ($m = 4$) also remains dominant in R4L3-MCS (see helical right-winding shape in (a2)) but becomes already strong modulated due to increased minor L3 contribution with $m = 3$ (see figure 7(2), there are still four pairs of vortex tubes but not symmetrically arranged anymore). It follows that the structure becomes more and more deformed. Visible is the isovorticity surface for $\eta = 80$ (red (dark gray)), it is narrow but still remains closed, whereas the one for $\eta = -80$ (yellow (light gray)) is already broken up. This means that the maximal vorticity at this position is decreased. Thus, the vortex intensity becomes weaker. Figure 7(3) presents the R4L3-/L3R4-MRIB with almost equal dominant mode amplitudes of both SPI contributions. Depending on the axial position, this solution indicates more right- or left-winding characteristics (b3). Note that (3) does not present a ‘perfect’ MRIB, due to ‘imperfections’, i.e. different amplitudes in the higher harmonic modes. Thus, the top of (b3) offers a more pronounced R4 contribution while the bottom one suggests the L3 contribution to be dominant. Note that only considering the (r, θ) plots the helicity, i.e. the winding characteristic of the flow is indistinguishable. Even while the isosurfaces in (4) are still open, the plot suggests a helical left-winding shape characterizing the dominant L3 contribution. The still strong but now only minor R4 contribution only results in strong modulation. Finally, the minor R4 contribution vanishes at the bifurcation point and thus (5) shows a pure L3-SPI with only azimuthal wavenumber $m = 3$.

5.3. Spatio-temporal behavior of transients

In order to illustrate the different structures appearing during the transition from 3-SPI to 4-SPI discussed in the previous section, we choose parameters for which L3R4-MCS but *no* R4L3-MCS (due to their major and minor contribution) stable exist, starting in an R4-SPI state (see figure 6(a), region E). To that end the preparation of R4-SPI as initial state was done by first confining to the subspace of R4-SPI and then releasing this confinement after a sufficient long relaxation time τ_D about 0.5 (see figure 8) in the remainder of the simulations. Note that not all constrictions are reversed, moreover, the solutions are confined to the subspace of MCS solutions. In this, in particular, R4-SPI, L3-SPI, R4L3-MCS, L3R4-MCS and R4L3-/L3R4-MRIB are able to exist. In doing so, one observes MCSs as bridging states during their transients to the respective final state (here L3R4-MCS) and thereby offering equal flow pattern as for the case of stable footbridge solutions. Here the full transformation reads R4-SPI \rightarrow R4L3-MCS \rightarrow R4L3/L3R4-MRIB \rightarrow L3R4-MCS.

5.3.1. Time evolution of modes and energy. Figure 8 depicts the time evolution of the dominant mode amplitudes $|u_{m,n}|$ after the preparation of unstable R4-SPI during the transformation scenario R4-SPI \rightarrow R4L3-MCS \rightarrow R4L3/L3R4-MRIB \rightarrow L3R4-MCS for control parameters $Re_1 = 370$ and $Re_2 = -550$ (region E in figure 6). After releasing the

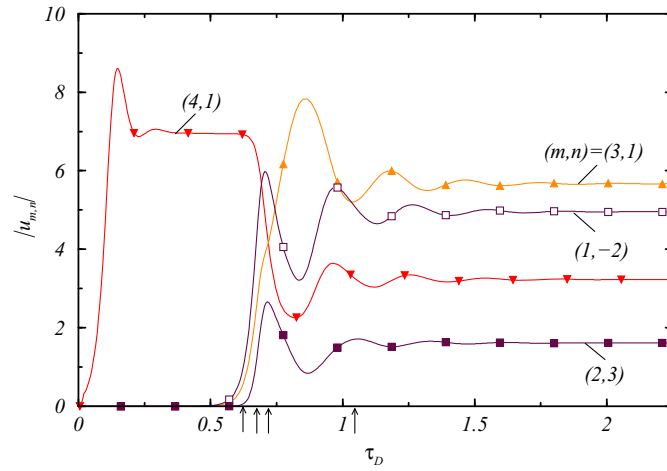


Figure 8. Time evolution of the (dominant) mode amplitudes $|u_{m,n}|$ during the transformation scenario R4-SPI→R4L3-MCS→R4L3-/L3R4-MRIB→L3R4-MCS at $Re_1 = 370$ and $Re_2 = -550$. Here the parameter lying in the region, where L3R4-MCS but *no* R4L3-MCS states stable exist (region E in figure 6(a)). The initial state was prepared by constricting the modes to the subspace of R4-SPI. Additional to both major, (3,1) and minor, (4, -1), SPI contributions to complete the MCS, both the largest nonlinear driven modes (1, -2) and (2,3) are also presented. Arrows below the abscissa mark five different time positions for which snapshots are presented in figure 10 (see also movie3.avi, movie4.avi and movie5.avi, available from stacks.iop.org/FDR/46/025503/mmedia).

constriction to R4-SPI subspace (τ_D at about 0.5) and only allowing for MCS subspace, the system is driven away from the unstable R4-SPI solution by computer noise only. In this case, there appear during a narrow time interval about 0.4 diffusion time ($\tau_D \in [0.5; 0.9]$ in figure 8) the structures R4L3-MCS and R4L3-/L3R4-MRIB as transient short-live-time solution before the system finally relaxes into a L3R4-MCS. All in all, the flow structures change quite fast after releasing the constrictions of preparation scenario.

Furthermore the temporal evolution of the energy in the system is interesting. Here as global measure of the flow, we will use the modal kinematic energy

$$E = \int_0^{2\pi} \int_{-\Gamma/2}^{\Gamma/2} \int_{r_i}^{r_o} \mathbf{u}\mathbf{u}^* r \, dr \, dz \, d\theta, \quad (8)$$

where \mathbf{u} is the velocity field. As discussed solutions are time-dependent, the time-averaged kinetic modal energy \bar{E} of (8) is taken over a very long time (long enough, typically several diffusion times, so that the average does not change very much).

Figure 9 shows the evolution of E during the transition from R4-SPI to L3R4-MCS (see figure 8). After releasing the stabilizing constrictions, the total energy, E , decreases quite fast from the energy level of a pure 4-SPI, $\bar{E}_{4\text{-SPI}}$, even below the level of a pure 3-SPI, $\bar{E}_{3\text{-SPI}}$. Hereafter it settles down also quite fast to the level of L3R4-SPI, $\bar{E}_{\text{L3R4-MCS}}$ which lies between both SPI states. Note that $\bar{E}_{\text{L3R4-MCS}}$ and $\bar{E}_{\text{R3L4-MCS}}$ are identical. Even while the MCS is significantly more complex than the pure SPIs, its total energy is smaller than that of R4-SPI.

It is just coincidental that the energy level $\bar{E}_{\text{L3R4-MCS}}$ for the L3R4-MCS lies almost in the middle of those for pure SPI, $\bar{E}_{4\text{-SPI}}$ and $\bar{E}_{3\text{-SPI}}$. For several MCSs having other SPI

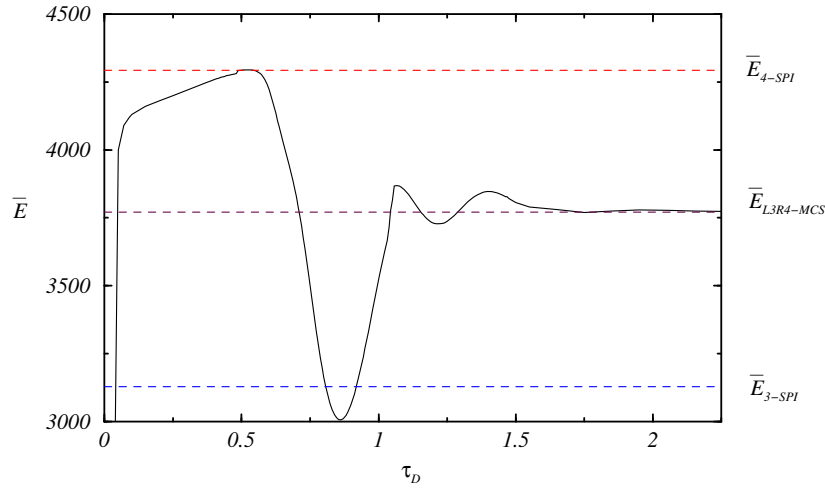


Figure 9. Variation of E with τ_D during the transformation from R4-SPI to L3R4-MCS at $Re_1 = 370$ and $Re_2 = -550$ (see figure 8). The dashed lines present the long-time averaged energies \bar{E} of flows as indicated.

contributions, we find the energy level to be independent of the SPI contributions; lying below, between or above that of the pure SPIs.

5.3.2. Spatio-temporal connections of transients. In order to follow the spatio-temporal changes, during the transition from the R4-SPI to L3R4-MCS and the change in the helicity of the flow structure, we made snapshots for five different time positions marked by arrows in figure 8 at $t_1 = 0.64$, $t_2 = 0.68$, $t_3 = 0.72$, $t_4 = 1.04$ and $t_5 = 2.25$. The flow pattern is shown in figure 10 depicting cuts in (r, θ) plane (a) at mid-height including the color-coded azimuthal vorticity η , isosurfaces of $\eta = \pm 80$ (b) and the radial velocity $u(d/2, \theta, z)$ (c) on an unrolled cylindrical surface in the annulus at mid-gap. Further details of the transformation R4L3-MCS \rightarrow R4L3/L3R4-MRIB \rightarrow L3R4-MCS can be seen in the online available material movie3.avi, movie4.avi and movie5.avi (available from stacks.iop.org/FDR/46/025503/mmedia).

After preparing the initial R4-SPI state due to constriction to the corresponding subspace, R4L3-MCS at t_1 is established relatively fast after releasing the constrictions. Here the helicity of the structure is still given by the major R4 contribution with its dominant $(4, -1)$ mode and just modulated by the minor L3 contribution with dominant $(3, 1)$ mode (see continuous contours (figure 10(c1)), $u = 0$, closed from top right to bottom left). The complete structure propagates downward. The minor contribution part results in local shrinking and expansion of the vortex tubes which remain helical right-winding orientated but visibly deformed by an upward propagating modulation. For later time t_2 the modulation in the $u = 0$ contours is increased, but the structure remains still helical right-winding orientated due to the major R4 contribution. It follows that the flow structure develops a stronger axial dependence. This situation begins to change at t_3 as the dominant mode amplitudes of both SPI contributions, $(3, 1)$ and $(4, -1)$, to conglomerate the MCS state become almost identical. This is the case of a R4L3-/L3R4-MRIB solution. Note that higher nonlinear stimulated mode amplitudes are not all identical and therefore there is no ‘perfect’ MRIB at t_3 . The higher modes of the R4 contribution are still more pronounced resulting in visible right-winding characteristics.

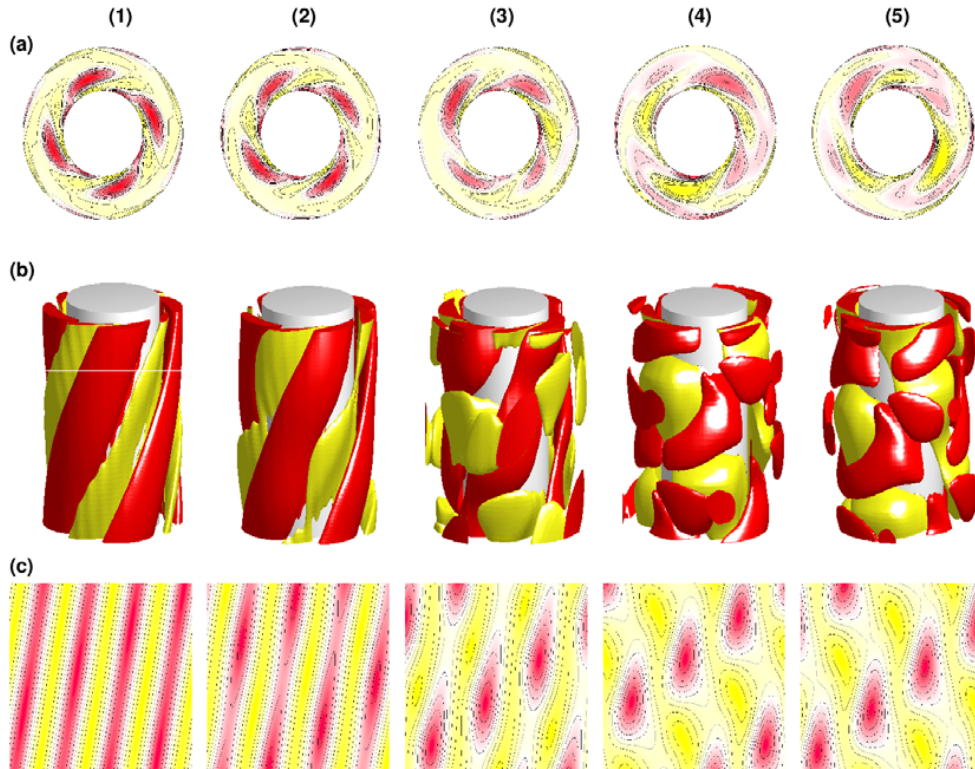


Figure 10. Snapshots of flow structures at five time positions $t_1 = 0.64$, $t_2 = 0.68$, $t_3 = 0.72$, $t_4 = 1.04$ and $t_5 = 2.25$ as marked by arrows at the abscissa in figure 8 during the temporal evolution R4L3-MCS \rightarrow R4L3-/L3R4-MRIB \rightarrow L3R4-MCS at $Re_1 = 370$ and $Re_2 = -550$. (a) Cuts at in (r, θ) plane at mid-height including the azimuthal vorticity η , color-coded from yellow (light gray) (minimum) to red (dark gray) (maximum). (b) Snapshots of the isosurfaces of the azimuthal vorticity $\eta = \pm 80$ [min, max] = [-350, 350]. Red (dark gray) (yellow (bright gray)) coloring denotes positive (negative) vorticity. In axial direction each isosurface plot covers one axial wavelength. (c) Radial velocity $u(d/2, 0, \theta, z)$ on an unrolled cylindrical surface in the annulus at mid-gap. Red (dark gray) (yellow (light gray)) denotes maximal inflow (outflow). For further details see also movie3.avi, movie4.avi and movie5.avi (available from stacks.iop.org/FDR/46/025503/mmedia).

From t_3 to t_4 the shape of the structure changes due to the exchange in the dominant SPI contributions, from R4 to L3. At t_4 a dominant helical left-winding orientation is obvious (see contours in u in figure 10(c4), there are closed ones now from top left to bottom right). This helical shape is further enforced until reaching the end state L3R4-MCS at t_5 , now with obvious major L3 and minor R4 contribution. The change of the azimuthal wave number can be followed in the (r, θ) plane (see figure 10(a)). Starting with four pairs of vortex tubes at t_1 due to major R4 contribution in the R4L3-MCS, one of these tubes becomes eliminated during evolution from t_2 to t_4 . Finally, at the end t_5 there are three pairs of vortex tubes. Note that these are more or less pronounced due to the strong modulation of the flow in axial direction.

Figure 11 summarizes the full scenario of MCSs establishing a footbridge solution in a schematic bifurcation diagram of vortex flow amplitudes versus control parameter, e.g. Re_2 (see also figure 4). The two different helical SPI solution branches with different azimuthal

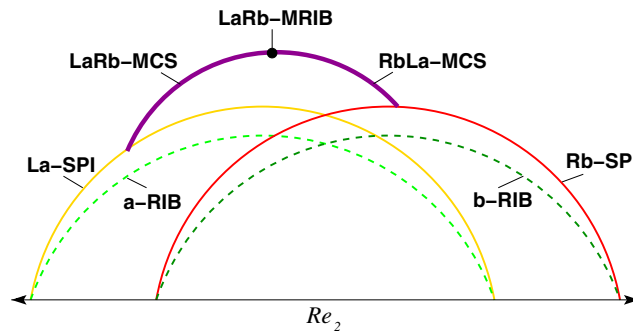


Figure 11. As figure 4: schematics for the bifurcation of vortex flow amplitudes versus a suitable control parameter, e.g. Re_2 . The azimuthal wave numbers of both SPI states are considered to be different $a \neq b$. MCSs establish footbridges that connect the Rb-SPI with the La-SPI solution branch. Note that the lines do not say anything about the stability of the respective solutions.

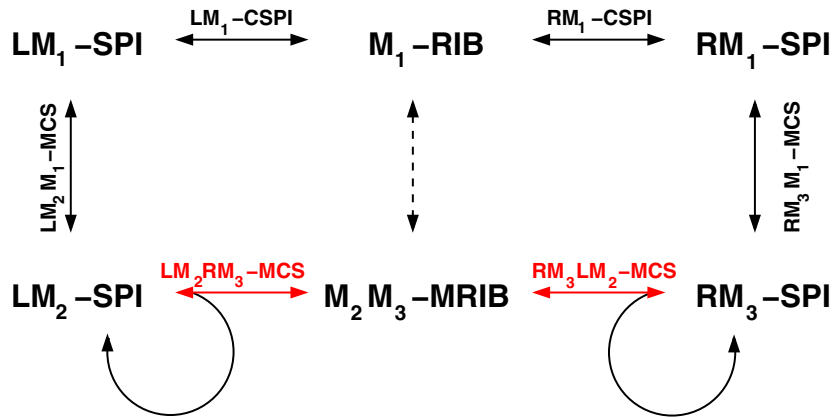


Figure 12. Schematics for the transitions between SPIs with azimuthal wave numbers M_i and either left(L)- and right(R)-winding helicity. Here $M_1 \neq M_2 \neq M_3$. The bottom level indicates the footbridge solutions (red (light gray) highlighted) investigated in this paper. The circles at the bottom indicate MCSs as bypass solutions (Altmeyer and Hoffmann 2010).

wave numbers $a \neq b$ are connected by footbridge solution of RaLb-/LbRa-MCS. In between for identical major and minor contributions a LaRb-/RbLa-MRIB solution exists. As in figure 4, the line style does not say anything about the stability of the respective solutions. But note that in contrast to MCS appearing as bypass solution for MCSs which establish footbridge solutions, it is *not* necessary for both SPI contributions to generate the MCS solution to exist simultaneously. Such scenarios have also been observed but just presenting a special case of a footbridge solution. Additionally, we also want to mention that we found such MCS bifurcating out of that SPI characterizing the minor contribution. Likewise the visualization of MCS branch above that of SPI does not say anything about the magnitude of mode amplitudes; in general the mode amplitude of major SPI contribution decreases at the bifurcation to compensate the increase of the modes of minor SPI contribution.

6. Conclusion and discussion

In this paper we elucidated the connection between several helical SPIs which differ in helicity and pitch. We considered differentially rotating cylinders with axial periodic boundary conditions, fixed axial wave number $k = 3.927$ and fixed radius ratio 0.883. The transition between different SPIs is mediated by secondarily bifurcating MCSs. We find these MCSs exhibit a *direct* way to establish stable footbridges between SPIs without involving further primary bifurcating solutions such as RIBs. RIBs play a crucial role in the transition scenario via wavy vortices (Hoffmann *et al* 2009).

For qualitative and quantitative analysis, we focused exemplarily on the transformation from R4-SPI to L3-SPI (due to symmetries the transformation from L4-SPI to R3-SPI is included) and investigated the bifurcation scenario and the spatio-temporal behavior of all states appearing therein. We were able to follow in detail how the vortex tubes of initial pure right-winding R4-SPI become destroyed and continuously stronger modulated and deformed due to decreasing R4 and increasing L3 contribution in the secondarily bifurcating R4L3-MCS. Approaching the R4L3-/L3R4-MRIB with almost identical R4- and L3-SPI contributions but opposite helicities the vortex tubes brake up. Passing the MRIB state, they reconnect again to result in helicity and propagation direction of the L3R4-MCS solution which is opposite to the former situation of R4L3-MCS. In the absence of any symmetry breaking effect, the transformation is reversible from L3-SPI to R4-SPI in the above-described scenario.

Flow states of MCSs as footbridges can appear either stale or unstable. Transient states elucidate similar spatio-temporal characteristics. To trace these transients, we applied some mode constrictions to find solutions in subspaces which are normally unstable in the full space. Letting fall some constrictions, we could follow the transient dynamics of footbridge solutions. Note that any solutions found in subspace are necessarily also solutions of the full space and hence represent physical flow states.

Finally, figure 12 elucidates schematics of the complete bifurcation scenario for MCS solutions. Three different kinds of bifurcations connecting different spirals are possible:

- (i) The transition between SPIs with the same azimuthal wavenumber M_1 but different helicities (Pinter *et al* 2006), L- an R- (top in figure 12). This is the special case of CSPI.
- (ii) The transition between SPIs with different azimuthal wave numbers $M_2 \neq M_3$ and also different helicities (bottom level). This is the new and main contribution of the present study (bottom in figure 12: red (light gray) highlighted footbridges).
- (iii) The transitions between SPIs with equal helicity but different azimuthal wave numbers (Deguchi and Altmeyer 2013) (left and right side in figure 12).

In addition, as a special case of the scenario (ii) one also finds MCS appearing as bypass solution (Altmeyer and Hoffmann 2010) starting and ending in the same SPI branch (circles on the bottom level).

We want to mention that one significant difference between MCS as bypass and MCS as footbridge solutions is that the latter can also appear *below* the bifurcation thresholds of the SPI contributions that generate the MCS.

Acknowledgment

I would like to thank my former co-supervisor Dr Ch Hoffmann for very good support and many fruitful discussions.

References

- Altmeyer S and Hoffmann Ch 2010 Secondary bifurcation of mixed-cross-spirals connecting travelling wave solutions *New J. Phys.* **12** 113035
- Andereck C D, Liu S S and Swinney H L 1986 Flow regimes in a circular Couette system with independently rotating cylinders *J. Fluid Mech.* **164** 155
- Chossat P and Iooss G 1994 *The Couette–Taylor Problem* (Berlin: Springer)
- Deguchi K and Altmeyer S 2013 On fully nonlinear mode competitions of nearly bicritical spiral or Taylor vortices in Taylor–Couette flow *Phys. Rev. E* **87** 043017
- DiPrima R C and Swinney H L 1985 Instabilities and transition in flow between concentric rotating cylinders *Hydrodynamic Instabilities and the Transition to Turbulence (Topics in Applied Physics vol 45)* ed H L Swinney and J G Gollub (Berlin: Springer) pp 139–80
- Golubitsky M and Stewart I 1986 Symmetry and stability in Taylor–Couette flow *SIAM J. Math. Anal.* **17** 249–88
- Golubitsky M, Stewart I and Schaeffer D G 1988 *Singularities and Groups in Bifurcation Theory* vol II (Berlin: Springer) pp 485–512
- Hoffmann C and Lücke M 2000 *Spiral Vortices and Taylor Vortices in the Annulus Between Counter-Rotating Cylinders* (Berlin: Springer) p 55
- Hoffmann Ch, Altmeyer S, Pinter A and Lücke M 2009 Transitions between Taylor vortices and spirals via wavy Taylor vortices and wavy spirals *New J. Phys.* **11** 053002
- Iooss G 1986 Secondary bifurcations of Taylor vortices into wavy inflow or outflow boundaries *J. Fluid Mech.* **173** 273–88
- Jones C A 1984 The transition to wavy Taylor vortices *J. Fluid Mech.* **157** 135
- Langford W F, Tagg R, Kostelich E J, Swinney H L and Golubitsky M 1988 Primary instabilities and bicriticality in flow between counter-rotating cylinders *Phys. Fluids* **31** 776
- Marques F and Lopez J M 2002 Modulated Taylor–Couette flow: onset of spiral modes *Theor. Comput. Fluid Dyn.* **16** 59
- Nagata M 1986 Bifurcations in Couette flow between almost co-rotating cylinders *J. Fluid Mech.* **169** 598
- Pinter A, Lücke M and Hoffmann Ch 2006 Competition between traveling fluid waves of left and right spiral vortices and their different amplitude combinations *Phys. Rev. Lett.* **96** 044506
- Pinter A, Lücke M and Hoffmann Ch 2008 Bifurcation of standing waves into a pair of oppositely traveling waves with oscillating amplitudes caused by a three-mode interaction *Phys. Rev. E* **78** 015304
- Swinney H and Gollub J 1981 *Hydrodynamic Instabilities and the Transition to Turbulence* (Berlin: Springer)
- Swift J, Gorman M and Swinney H 1982 Modulated wavy vortex flow in laboratory and rotating reference frames *Phys. Lett. A* **87** 457
- Taylor G I 1923 Stability of a viscous liquid contained between two rotating cylinders *Phil. Trans. R. Soc. A* **223** 289
- Tagg R 1994 The Couette–Taylor problem *Nonlinear Sci. Today* **4** 1